THE EFFECT OF MIXING ON THE METASTABLE ZONE WIDTH AND NUCLEATION KINETICS IN THE ANTI-SOLVENT CRYSTALLIZATION OF BENZOIC ACID

D. O'Grady, M. Barrett, E. Casey and B. Glennon*

School of Chemical and Biochemical Engineering, University College Dublin, Belfield, Dublin, Ireland.

Abstract: The effects of anti-solvent addition rate and location, and agitation speed on the metastable zone width of an anti-solvent system were investigated using focused beam reflectance measurement (FBRM) and attenuated total reflectance-Fourier transform infra-red spectroscopy. Benzoic acid in ethanol-water mixtures, with water acting as anti-solvent, was chosen as the model system and was studied at a 500 mL scale. FBRM proved to be the more sensitive method for the detection of nucleation onset. In general, the metastable zone widened with increasing addition rate, with the effect most pronounced when the anti-solvent was added close to the impeller. At this location, an increase in agitation intensity resulted in a narrower metastable zone for all addition rates. For an addition location close to the vessel wall, the metastable zone was narrower and the impact of addition rate and agitation were less pronounced. Substantial variation in the measured metastable zone width was also observed, with nucleation occasionally occurring at bulk concentrations less than the saturation level. It is proposed that the metastable zone width is influenced by the differing degrees of anti-solvent incorporation at each addition location. Close to the impeller anti-solvent is rapidly incorporated leading to consistent results, but, close to the vessel wall, incorporation is hindered by unfavourable mixing conditions leading to premature nucleation and more variability. Computational Fluid Dynamics simulations support this observation. Using the measured metastable zone widths, nucleation kinetics at two different agitation intensities were estimated. Using this data, an agitation dependent expression for the nucleation rate was generated.

Keywords: anti-solvent crystallization; metastable zone width; nucleation.

**Correspondence to:*
Dr B. Glennon, School of Chemical and Biochemical Engineering, University College Dublin, Belfield, Dublin 4, Ireland.
E-mail: brian.glennon@ucd.ie

DOI: 10.1205/cherd06207

0263–8762/07/
$30.00 + 0.00

Chemical Engineering Research and Design

Trans IChemE,
Part A, July 2007

INTRODUCTION

The addition of an anti-solvent to a concentrated solution to induce crystallization of the solute through a reduction in its solubility in the combined solvent mixture is a powerful isolation and purification technique, particularly for systems in which the temperature coefficient of solubility is low or the solute is unstable at elevated temperatures. Its use in the crystallization of pharmaceutical compounds is, therefore, common. Particular problems associated with anti-solvent crystallization include wide batch-to-batch variability, fine and irregularly shaped product crystals and solvate/hydrate formation. The effects of various process parameters, including type of anti-solvent (Takiyama *et al*., 1998; Oosterhof *et al*., 1999), feed concentration (Holmbäck and Rasmuson, 1999; Barata and Serrano, 1998) solution concentration (Kaneko *et al*., 2002; Kitamura and Sugimoto, 2003), anti-solvent addition rate (Beckmann, 1999; Holmbäck and Rasmuson, 1999) and agitation intensity (Takiyama *et al*., 1998, Yu *et al*., 2005), on the size, number, shape, degree of agglomeration and polymorphic form of product crystals have been reported. However, less attention has been paid to the metastable zone width and its relationship with the process conditions (Guo *et al*., 2005; Pina *et al*., 2001).

The metastable zone width (MSZW) is an extremely important parameter in the design and optimization of crystallization processes. A solute will remain in solution until a sufficiently high level of supersaturation is generated to induce spontaneous nucleation. Typically, it is desirable to operate away from this metastable limit so as to ensure reliable process performance. Metastable zone information can be used to optimise crystallization processes (Ulrich and Strege, 2002) and calculate nucleation kinetics (Nyvlt, 1968). The MSZW may be affected by various process parameters, such as supersaturation generation rate (Barrett and Glennon, 2002), agitation speed (O'Sullivan,

2005) and the presence of impurities (Myerson & Jang, 1995; Sayan and Ulrich, 2001).

Recent research aimed at modelling the impact of mixing on crystallization has focused on reactive crystallization (Tavare, 1995; Phillips *et al*., 1999; David, 2001; Torbacke and Rasmusson, 2004). Little work has been conducted studying the impact of mixing on the MSZW for anti-solvent systems. Mixing is critical for all crystallization systems but in the case of anti-solvent addition adequate mixing is needed to incorporate the anti-solvent into the bulk solution and maintain a constant level of supersaturation throughout the crystallizer, over a potentially wide volume range. This must be achieved while considering many other mixing sensitive parameters such as solids suspension, attrition, impurity profile, agglomerate formation/break-up, of entrainment of gas/vapour from the headspace and rate of heat transfer (Paul *et al*., 2005, Woo *et al*., 2006). In this work, the effect of addition rate, agitation speed and feed point location on MSZW are investigated at a 500 mL scale. Focused beam reflectance measurement (FBRM) and attenuated total reflectance-Fourier transform infra-red (ATR-FTIR) spectroscopy are implemented to detect nucleation. Computational fluid dynamics (CFD) software is used to model the mixing behaviour of the systems under investigation and to provide an explanation of the observed results.

FBRM is a probe-based instrument that measures a function of the size, shape and population of a particulate system in-process and in real time. It can measure the degree of change to these properties as well as the rate of change making it a useful tool for the study of dynamic particulate systems. Its advantage over other off-line techniques is that it measures the particles *in situ*, eliminating the need to sample and ensuring that the particles are measured under process conditions. In this work, it is used to detect the onset of nucleation as the first particles appear in the system.

FBRM operates by shining a monochromatic laser beam, of wavelength 790 nm, generated by a class 1 laser source, via a fibre optic conduit, to an optical assembly housed within a probe shaft. This optical assembly, which consists of a lens mounted eccentrically, rotates in a circular motion at high speeds. The circular motion is generated mechanically in the model used for this work (S400A). For the duration of this work, the scan speed was held constant at 2 ms^{-1} at which the effective measurement range is between 0.5 and 1000 μm. At higher scan speeds the measurement range can be extended at the upper level but in doing so the sensitivity at the lower end of the range is compromised. As the monochromatic beam passes through the lens it is focused to a fine point ($d \sim 4$ μm) just inside the probe window. The circular motion of the assembly traces the fine point of the laser over the circumference of a circle. When the beam comes in contact with a particle, light is reflected in all directions. Some of the light is reflected back up the probe to a detector. The detector measures the time duration for which the light is reflected. This time duration can be used to measure a chord length across the particle. This data can then be classified into a range of chord sizes from 0 to 1000 μm. A more detailed description of how FBRM operates can be found in the literature (Barrett and Glennon, 2002).

ATR-FTIR spectroscopy measures solution concentration by irradiating the solution with infrared light to produce an infrared spectrum. This spectrum is characteristic of the vibrational structure of the substance in immediate contact with the ATR probe and can be described as a unique 'fingerprint' of the liquid phase. An ATR crystal is chosen so the depth of penetration of the infrared energy is smaller than the liquid phase barrier between the probe and the solid crystal particles, leading to its increasing popularity as a monitoring technique in crystallization processes (Fujiwara *et al*., 2002; Liotta and Sabesan, 2004; Yu *et al*., 2006). Hence when the probe is inserted into a crystal slurry the probe should be in immediate contact with the liquid phase and interference from the solid phase should be negligible. Despite this assumption some researchers have noted interference of the spectrum by the solid phase in crystallization systems (O'Sullivan, 2005). The liquid phase concentration is a function of the infrared spectrum generated and a calibration model is used to interrelate the data. A more detailed description of spectroscopy in general and the mode of operation of the ATR-FTIR probe is available elsewhere, (O'Sullivan, 2005).

CFD have been used to model semi-batch reactive crystallizations and has been used to predict the effect of mixing on the supersaturation distribution and the resulting size of the crystals (Wei *et al*., 2001; Baldyga and Orciuch, 2001). It has also been used to study the effect of mixing on product yield (Akiti and Armenante, 2004). CFD has also been used in conjunction with crystallization kinetics and solubility data to simultaneously solve the mass and population balances for a reactive crystallization, allowing the impact of feed rate, agitation intensity, feed point and feed tube diameter on nucleation rate and crystal size to be illustrated (Zauner and Jones, 2002).

With accurate MSZW information it is possible to estimate nucleation kinetics. This is achieved by modifying classical nucleation theory (Nyvlt, 1968) for an anti-solvent system. Much of the literature focuses on static induction time experiments to estimate nucleation kinetics for an anti-solvent system (Barata and Serrano, 1996). However useful nucleation kinetics can be gathered using dynamic experiments and this method will be used here.

METHODS AND MATERIALS

Benzoic acid is soluble in ethanol and essentially insoluble in water (58.36 g and 0.25 g respectively in 100 g at 25°C (O'Grady, 2007). For the work reported here, all measurements were made at 25°C (see Table 1 for data).

An initially undersaturated solution, containing 75 g water, 75 g ethanol and 21 g benzoic acid, was held at 25°C in a 500 mL glass jacketed vessel with a Julabo chiller fitted for temperature control. A motor driven, pitched blade impeller

Table 1. Measured solubility data for benzoic acid-ethanol-water systems (O'Grady, 2007).

g water/g ethanol	g benzoic acid/g ethanol
1.01	0.41
1.4	0.29
1.8	0.21
2.2	0.15
2.73	0.1

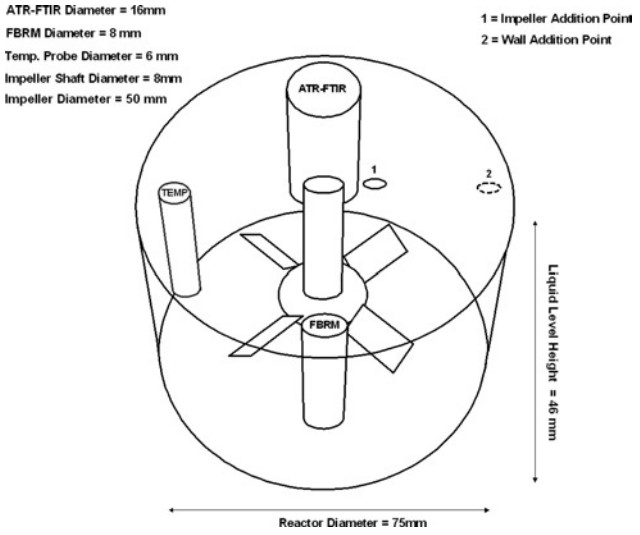

Figure 1. Crystallizer configuration.

provided agitation. FBRM (S400 A; Mettler Toledo), ATR-FTIR (ReactIR 4000; Mettler Toledo) and temperature probes were placed in the vessel to monitor the crystallization. Although the vessel was not baffled, the probes were considered sufficient to ensure good mixing (see Figure 1). Water at 25°C was fed to the vessel at a variety of addition rates (0.05 g s^{-1}, 0.14 g s^{-1}, 0.24 g s^{-1}, 0.34 g s^{-1} and 0.48 g s^{-1}). Two addition locations (see Figure 1) and two agitation intensities (325 rpm and 475 rpm) were investigated. All additions are above surface. The impeller shaft is 10 mm above the base of the vessel, and the tips of all probes are in a plane 2 mm above the top of the impeller. All experiments were performed in triplicate and the reported values are the mean of the three experiments. The error bars reported are for the standard deviation on the mean.

Computational Fluid Dynamics

To investigate the velocity profiles prior to nucleation, the system is treated as a single phase and the possible solid-liquid interactions after nucleation are not considered. Initially, the 500 mL vessel and its complex baffling system (the FBRM, REACT-IR and temperature probes) are modelled within GAMBIT 2.1.6. Details are given in Figure 1. GAMBIT is a software package designed to aid in the construction and meshing of systems for CFD applications. The precise geometry and dimensions of the system (pitch blade impeller, probes and so on) are created in the graphical user interface allowing for the meshing of the vessel and its internals, along with the assigning of zone types and system specifics (i.e., fluid viscosity, internal reactor temperature and agitation speed).

A large number of individual volumes created in the construction of the geometry are then meshed. The system contains 823 individual volumes and ~475 000 cells. An unstructured hexahedral meshing scheme is applied, as less numerical diffusion errors are evident then in a tetrahedral-based mesh. The mesh created in GAMBIT is then exported to FLUENT 6.1.22 for solution of the momentum and continuity equations for the turbulent flow within the crystallizer. The 'multiple reference frame' (MRF) approach is applied to the system and the flow equations solved using the SIMPLE algorithm. The Reynolds number for the agitation speeds assessed lies between ~12 500 (325 rpm) and ~18 500 (475 rpm). The standard $k-\varepsilon$ turbulence model was chosen to model the flows. In addition, a no-slip boundary condition was imposed on all walls and the free liquid surface was modelled with no vortex, a zero-flux and zero-stress conditions. To validate the model the tip speed of the impeller is calculated and compared to the tip speed calculated using the model. The model underestimated the tip speed by about 3% at 325 and 475 rpm.

RESULTS AND ANALYSES

Comparison of FBRM and ATR-FTIR Methods for the Detection of Nucleation

FBRM and ATR-FTIR detect the formation of crystals in different ways. FBRM detects the point at which crystals are initially apparent in the solution, whereas ATR-FTIR detects the point at which the solution concentration starts to decrease, indicating solute is being forced out of solution and crystals are being formed. To measure the actual solution concentration a calibration model is needed, but for the purpose of identifying the point of nucleation such a model is not necessary, since it is sufficient to examine peaks in the spectrum associated with benzoic acid.

Figure 2 shows a waterfall plot for a typical crystallization. The peak at 1275 cm^{-1} represents the C-O bond present in the benzoic acid molecule. The peak at 1480 cm^{-1} is representative of a C-C bond indicating an aromatic group. After a 10-min hold period to equilibrate the temperature, water is added, in this case, at 0.045 g s^{-1} (and agitation speed of 475 rpm). Examining the peak at 1275 cm^{-1} the concentration of benzoic acid in solution decreases at a steady rate due to dilution. After about 5 min there is a sharp decrease in this peak, indicating that the concentration of benzoic acid in solution is decreasing at a faster rate due to the formation of benzoic acid crystals. In this way the onset of nucleation can be identified using ATR-FTIR with no need for a calibration model.

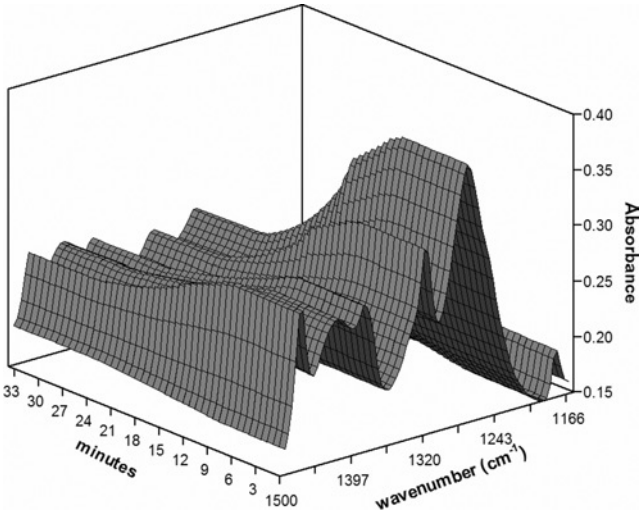

Figure 2. ATR-FTIR waterfall plot for standard MSZW experiment. This figure is available in colour online via www.icheme.org/cherd

To compare the FTIR results with those obtained using FBRM, the chord length distributions were measured (on a 10 s measurement duration) over the same time period. It was noted that the counts per second data in the region 0–10 μm exhibited more noise than the counts data in the 10–100 μm region. Therefore, the count rate in the latter region was used for nucleation detection. The chosen range also ensured that agglomerates of newly formed crystals were also detected. In general, however, it is advisable to chose the most sensitive detection range by inspection. Figure 3 shows the comparison between FBRM counts (10–100 μm), and the height of the benzoic acid IR absorption peak at 1275 cm^{-1}. By the nature of its operation, the FBRM indicates clearly the point at which it first detects crystals in the system. The FTIR system, on the other hand, responds to the formation of crystals when the solute concentration has fallen by a detectable amount. Figure 4 focuses on the region where nucleation occurs and shows that FBRM detects the onset of nucleation before the ATR-FTIR. For each of the three addition rates investigated, the FBRM detected the point of nucleation before the ATR-FTIR (see Figure 5), with the difference most pronounced at higher addition rates. The points of nucleation were determined by visual inspection of the unsmoothed, unfiltered data. The shorter sampling time (2 s compared to 30 s) and a greater sensitivity to the small system changes during the onset of nucleation contribute to this difference. For this reason, FBRM was chosen as the method of choice for detection of the point of nucleation.

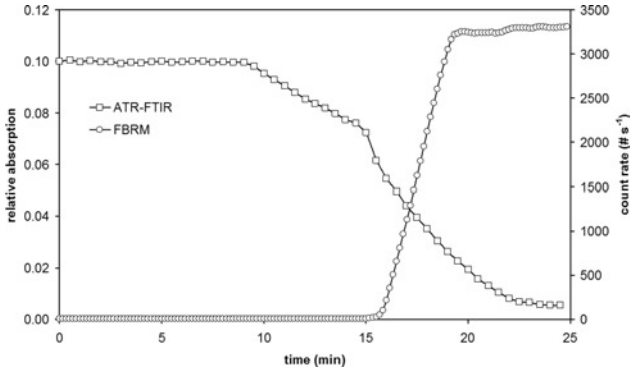

Figure 3. Profile for FBRM count rate (between 10–100 μm) and FTIR absorption peak height at 1275 cm^{-1}.

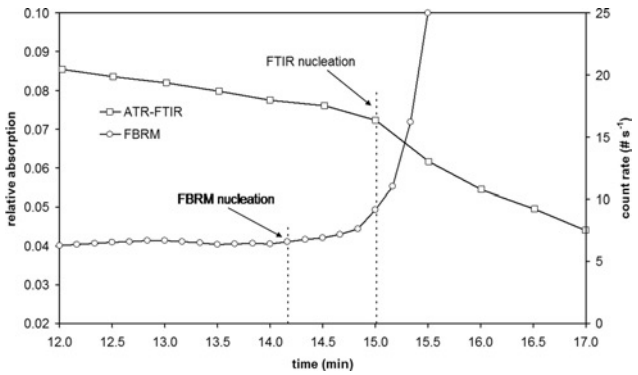

Figure 4. Point of nucleation determination using FBRM count rate (10–100 μm) and IR absorption peak height at 1275 cm^{-1}.

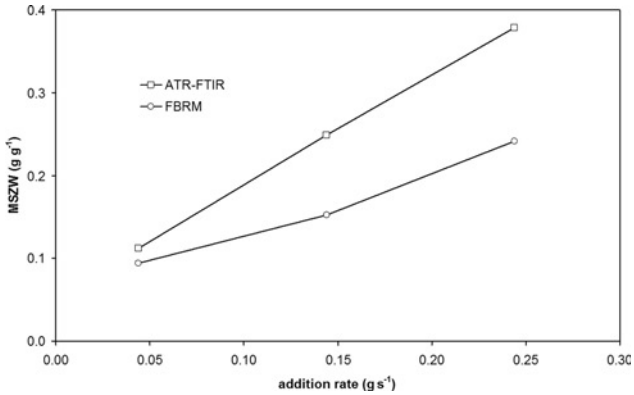

Figure 5. Comparison of MSZW (in terms of g water per g ethanol) measured by FBRM and ATR-FTIR.

Effect of Process Parameters

Figure 6 shows the impact of addition rate and agitation intensity on the MSZW when anti-solvent is added close to the impeller (addition point 1 in Figure 1). At a given agitator speed, the metastable zone becomes wider as the addition rate increases. This increase in MSZW with increasing supersaturation generation rate is typical of most crystallization systems (Barrett and Glennon, 2002).

For each addition rate studied, an increase in the agitation intensity results in a narrower metastable zone. Agitation can have two effects on the metastable zone width (Mullin, 2001). Increased agitation can narrow the MSZW by increasing the probability of solute molecules contacting to form the critical sized nuclei necessary for nucleation. However, this increase in agitation can also break up these clusters widening the MSZW. For an anti-solvent system there is the added factor of mixing between the solvent and anti-solvent. It may be expected that if agitation is not sufficient to rapidly disperse the anti-solvent, then locally high levels of supersaturation may develop, inducing nucleation at an earlier stage. There is, however, no evidence of such a trend for this addition location, suggesting that the bulk mixing is sufficient, while the increase in agitation intensity is increasing the probability of critical nuclei formation.

Similar experiments were performed with an addition point close to the wall of the vessel (addition point 2 in Figure 1).

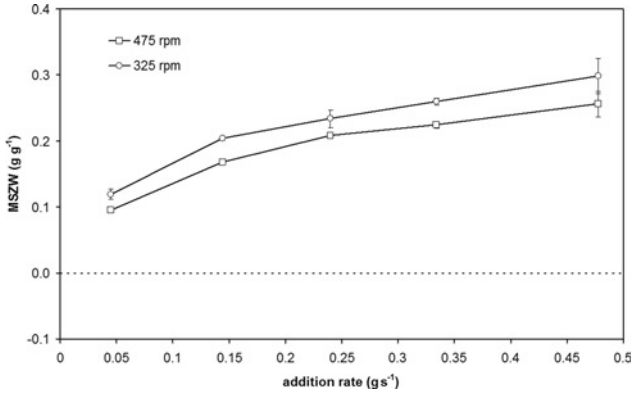

Figure 6. Variation in metastable zone width as a function of agitator speed and addition rate for an addition location close to the impeller.

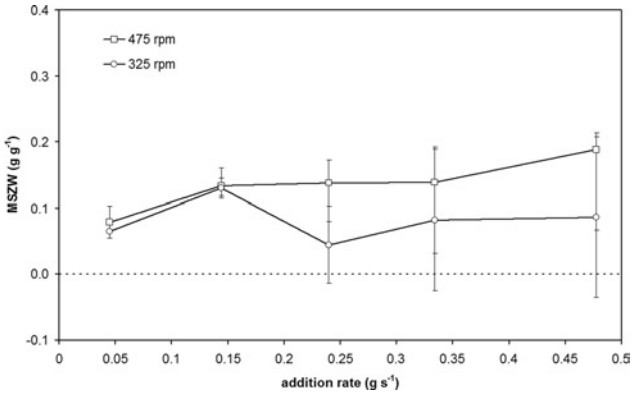

Figure 7. Variation in metastable zone width as a function of agitator speed and addition rate for an addition location close to the vessel wall.

For this operating configuration, the addition rate had substantially less effect on the metastable zone width, which did not exceed 0.2 g g^{-1} for any addition rate (see Figure 7).

In general, the MSZW is significantly narrower when the anti-solvent is added close to the wall. This can be explained by considering the unfavourable mixing conditions at the wall. Addition close to the impeller ensures rapid incorporation of the anti-solvent into the bulk solution, whereas addition close to the wall leads to areas of locally high supersaturation close to the addition location. There was also a far greater variability in the MSZW, especially at 325 rpm and at higher addition rates. It would appear that, in this set of experiments, incorporation of the anti-solvent into the bulk flow is the critical step in process. At high addition rates it becomes increasingly harder to incorporate the anti-solvent into the bulk solution, leading to the generation of locally high levels of supersaturation close to the feed point. This can result in early nucleation, often at bulk concentrations below the saturation level. Increasing the agitation facilitates dissipation of the local supersaturation resulting in a wider metastable zone and less variability in the results.

In order to investigate further the MSZW data collected here, CFD models of the flow fields in the vessel were completed as described above. Figures 8 and 9 depict velocity in the *z*-direction (parallel to impeller shaft) at the liquid surface for impeller speeds of 325 rpm and 475 rpm, respectively. Figures 10 and 11 depict velocity in the *z*-direction through a cross section of the vessel for impeller speeds of 325 rpm and 475 rpm, respectively. Velocity in this direction was chosen for inspection, as it will impact on the incorporation of the anti-solvent into the bulk of the vessel. It is clear that, close to the impeller, the velocity is in the downward direction, but close to the wall the velocity is in the upward direction. Therefore, when anti-solvent is added close to the impeller it is incorporated easily into the bulk solution. However, when it is added close to the wall this incorporation is more difficult. This may lead to an area of local supersaturation close to the feed point and, hence, premature variable nucleation as observed experimentally.

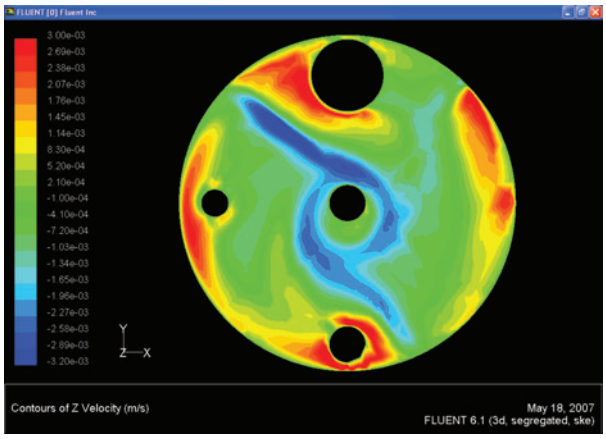

Figure 9. Predicted mean velocity in the *z*-direction at the liquid surface for an impeller speed of 475 rpm. This figure is available in colour online via www.icheme.org/cherd

Nucleation Kinetics

With sufficient metastable zone width data it is possible to calculate nucleation kinetics for the anti-solvent system. It is important to identify an operating regime where such kinetics may be reliably calculated. In the situation where anti-solvent

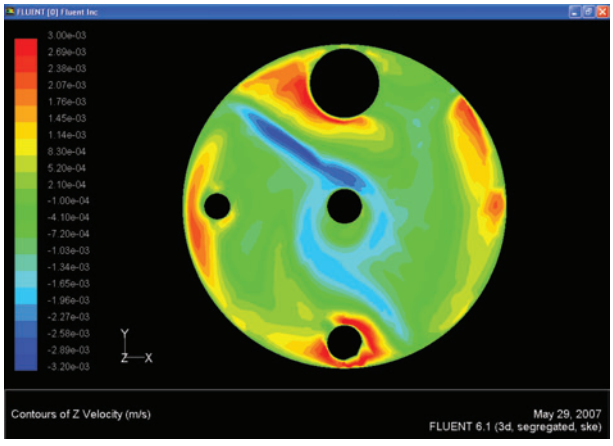

Figure 8. Predicted mean velocity in the *z*-direction at the liquid surface for an impeller speed of 325 rpm. This figure is available in colour online via www.icheme.org/cherd

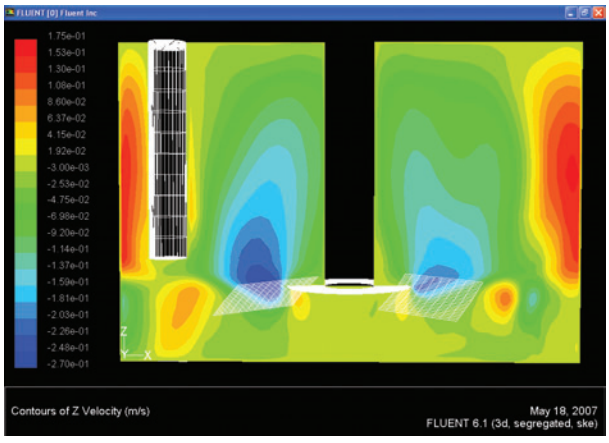

Figure 10. Predicted mean velocity in the *z*-direction through a cross section of the vessel for impeller speeds of 325 rpm. This figure is available in colour online via www.icheme.org/cherd

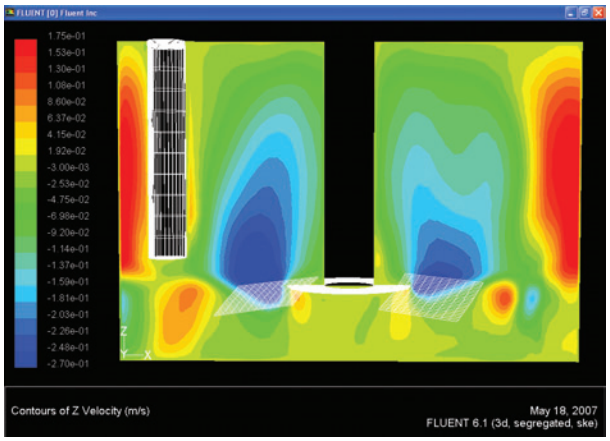

Figure 11. Predicted mean velocity in the *z*-direction through a cross section of the vessel for impeller speeds of 475 rpm. This figure is available in colour online via www.icheme.org/cherd

was added at the wall location, and at 325 rpm, it is probable that true nucleation kinetics cannot be estimated. This is because the observed nucleation occurs due to excessive local supersaturation near the addition point rather than true supersaturation in the bulk of the liquid. When the addition location is close to the impeller, the nucleation does not appear to be so dominated by the local hydrodynamic conditions. In this case useful kinetic information may be estimated.

Classical nucleation theory (Nyvlt, 1968) can be applied to the MSZW data as used with modifications for anti-solvent addition rather than cooling

$$J = k_o \Delta c^n \tag{1}$$

During anti-solvent addition, the rate of supersaturation generation can be expressed as a function of the specific anti-solvent addition rate

$$\frac{d\,\Delta c}{d\,t} = r\frac{d\,c^*}{d\,A} \tag{2}$$

At the point of nucleation, the supersaturation is related to the metastable zone width by

$$\Delta c_{max} = \Delta A_{max}\frac{dc^*}{dA} \tag{3}$$

where the metastable zone width is given by

$$A_{max} = A^* - A_{nuc} \tag{4}$$

O'Grady (2007) reports dc^*/dA equal to 0.2231 g solute g^{-1} solvent g^{-1} anti-solvent for the benzoic acid–ethanol–water system. At the point of nucleation, it may be assumed that the rate of supersaturation generation equals the rate of formation of new crystals which is given by

$$\frac{dM}{dt} = k_o k_v p_c r_{nuc}^3 \Delta c^n = k_n \Delta c^n \tag{5}$$

Combining equations (2), (3) and (5) yields

$$\ln(r) = (n-1)\ln\left(\frac{dc^*}{dA}\right) + \ln(k_n) + n\ln(\Delta A_{max}) \tag{6}$$

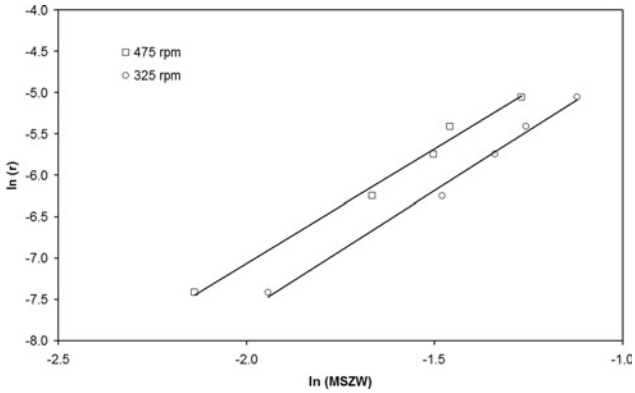

Figure 12. Nucleation behaviour at impeller speeds of 325 and 475 rpm.

Using equation (6), the nucleation kinetic parameters can be readily obtained from the reported metastable zone width data. As shown in Figure 12, the nucleation kinetics appear to be a function of the impeller speed.

Modifying equation (5) in the form

$$\frac{dM}{dt} = k_n' N^\alpha \Delta c^n \tag{7}$$

to incorporate the influence of agitation, the following modified version of equation (6) may be obtained

$$\ln(r) = (n-1)\frac{dc^*}{dA} + \ln(k_n') + n\ln(\Delta A_{max}) + \alpha\ln(N) \tag{8}$$

In this case, a non-linear regression analysis was completed to evaluate the parameters in equation (7) yielding the following expression

$$\frac{dM}{dt} = 0.1278\ N^{1.3}\Delta c^{2.9} \tag{9}$$

From equation (8), the metastable zone width can be obtained thus

$$\Delta A_{max} = \left(\frac{r}{k_n' N^\alpha}\right)^{1/n}\left(\frac{dc^*}{dA}\right)^{(1/n)-1} \tag{10}$$

Good agreement is obtained between the predictions of equation (9) and the experimental data (see Figure 13),

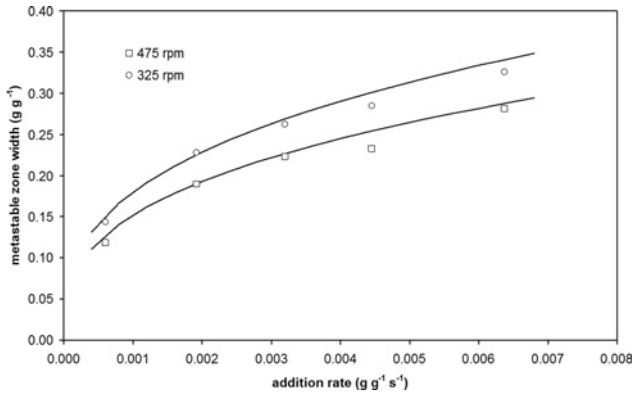

Figure 13. Metastable zone widths predicted from equation (9).

supporting the contention that impeller speed plays a critical role in determining the level of nucleation in the vessel, and thus providing a correlation to facilitate quantification of the role of impeller speed in the determination of nucleation rates. This is consistent with the observations made based on the measured trends in metastable zone width.

DISCUSSION AND CONCLUSIONS

The effect of addition rate and location, along with agitation intensity, on the metastable zone width has been investigated for an anti-solvent crystallization. An addition location close to the impeller results in a repeatable crystallization and a positive correlation between the addition rate and the MSZW. An addition location close to the wall of the vessel results in a significantly narrower MSZW, and more random nucleation behaviour.

The effect of agitation intensity depends on the addition location. When anti-solvent is added close to the impeller, an increase in agitation intensity results in a narrower MSZW, possibly due to the increased probability of contact between solute molecules. When anti-solvent is added close to the wall, an increase in agitation results in a wider MSZW and a significant improvement in the batch-to-batch repeatability. These results can be explained in terms of mixing conditions at each of the addition locations. Close to the impeller, mixing conditions allow for the rapid incorporation of the anti-solvent and a homogenous mixture of solution and anti-solvent. However, close to the wall, mixing conditions are less suitable and areas of supersaturation build up leading to narrower MSZWs and a reduction in the batch-to-batch repeatability. In this situation, when the agitation is increased, the local areas of supersaturation can be dissipated, to some degree, and the MSZW is wider and the batch-to-batch repeatability improves.

By modifying classical nucleation theory for an anti-solvent system, it was possible to estimate the nucleation order and the nucleation constant at both agitation intensities, and for the addition location close to the impeller. Only this location was studied as addition close to the wall resulted in unrepeatable experiments and nucleation was judged to be a result of local areas of supersaturation close to the addition location rather than as a result of supersaturation in the bulk solution. Agitation clearly impacted on the nucleation kinetics and to account for this the nucleation rate expression was modified, to account for agitation, and solved using a non-linear regression. The modified equation fitted the experimental data adequately.

NOMENCLATURE

A	anti-solvent concentration, g anti-solvent g^{-1} solvent
A^*	anti-solvent concentration at solute saturation, g anti-solvent g^{-1} solvent
A_{nuc}	anti-solvent concentration at point of nucleation, g anti-solvent g^{-1} solvent
c^*	saturated solute concentration, g solute g^{-1} solvent
J	nucleation rate, # m^{-3} s^{-1}
k_0	nucleation constant [equation (1)]
k_n	nucleation constant [equation (5)]
k'_n	nucleation constant [equation (7)]
k_v	volumetric shape factor
M	mass of nuclei formed, g m^{-3}
n	nucleation order
N	impeller speed, s^{-1}
r	specific anti-solvent addition rate, g anti-solvent/g solvent s^{-1}
r_{nuc}	nuclei radius, m
t	time, s
Δc	supersaturation, g solute g^{-1} solvent
α	exponent on impeller speed in equation (7)
ρ_c	crystal density, g m^{-3}

REFERENCES

Akiti, O. and Armenante, P.M., 2004, Experimentally-validated micromixing-based CFD model for fed-batch stirred-tank reactors, *AIChE J*, 50(3): 566–577.

Baldyga, J. and Orciuch, W., 2001, Some hydrodynamic aspects of precipitation, *Powder Tech*, 121(1): 9–19.

Barata, A. and Serrano, M.L., 1996, Salting out of potassium dihydrogen phosphate (KDP) II. Influence of agitation intensity, *J Crystal Growth*, 163(4): 426–433.

Barata, A. and Serrano, M.L., 1998, Salting out of potassium dihydrogen phosphate (KDP) IV. Characterization of the final product, *J Crystal Growth*, 194: 199–118.

Barrett, P. and Glennon, B., 2002, Characterizing the metastable zone width and solubility curve using Lasentec FBRM and PVM, *Trans IChemE Part A: Chem Eng Res Des*, 80: 799–805.

Beckmann, W., 1999, Nucleation phenomena during the crystallization and precipitation of Abecarnil, *J Crystal Growth*, 199: 1307–1314.

David, R., 2001, General rules for prediction of the intensity of micromixing effects on precipitations, *Powder Tech*, 121: 2–8.

Fujiwara, M., Chow, P.S., Ma, D.L. and Braatz, R.D., 2002, Paracetamol crystallization using laser backscattering and ATR-FTIR spectroscopy: metastability, agglomeration and control, *Crystal Growth & Design*, 2(5): 363–370.

Guo, Z., Zhang, M., Li, H., Wang, J. and Kougoulos, E., 2005, Effect of ultrasound on anti-solvent crystallization process, *J Crystal Growth*, 273: 555–563.

Holmbäck, X. and Rasmuson, A.C., 1999, Size and morphology of benzoic acid crystals produced by drowning-out crystallisation, *J Crystal Growth*, 199: 780–788.

Kaneko, S., Yamagami, Y., Tochihara, H. and Hirasawa, I., 2002, Effect of supersaturation on crystal size and number of crystals produced in antisolvent crystallization, *J Chem Eng Japan*, 35: 1219–1223.

Kitamura, M. and Sugimoto, M., 2003, Anti-solvent crystallization and transformation of thiazole-derivative polymorphs—I: Effect of addition rate and initial concentrations, *J Crystal Growth*, 257: 177–184.

Liotta, V. and Sabesan, V., 2004, Monitoring and feedback control of supersaturation using ATR-FTIR to produce an active pharmaceutical ingredient of a desired crystal size, *Org Proc Res Dev*, 8: 488–494.

Mullin, J.W., 2001, *Crystallization*, 4th edition (Butterworth-Heinemann, Oxford, UK).

Myerson, A.S. and Jang, S.M., 1995, A comparison of binding energy and metastable zone width for adipic acid with various additives, *J Crystal Growth*, 156: 459–466.

Nyvlt, J., 1968, Kinetics of nucleation in solution, *J Crystal Growth*, 3–4: 377–383.

O'Grady, D., 2007, Multiscale characterisation of anti-solvent crystallization, PhD thesis, University College Dublin, Ireland.

Oosterhof, H., Witkamp, G.J. and van Rosmalen, G.M., 1999, Some anti-solvents for crystallization of sodium carbonate, *Fluid Phase Equilibria*, 155: 219–227.

O'Sullivan, B., 2005, The application of in situ analysis to crystallization process development, PhD thesis, University College Dublin, Ireland.

Paul, E.L., Tung, H.H. and Midler, M., 2005, Organic crystallization processes, *Org Powder Tech*, 150: 133–143.

Phillips, R., Rohani, S. and Baldyga, J., 1999, Micromixing in a single-feed semi-batch precipitation process, *AIChE J*, 45: 82–92.

Pina, C.M., Fernandez-Diaz, L., Prieto, M. and Veintemillas-Verdaguer, S., 2001, Metastability in drowning-out crystallisation: precipitation of highly soluble sulphates, *J Crystal Growth*, 222: 317–327.

Sayan, P. and Ulrich, J., 2001, Effect of various impurities on the hardness of NaCl crystals, *Crystal Res and Tech*, 36(11): 1253–1262.

Takiyama, H., Otsuhata, T. and Matsuoka, M., 1998, Morphology of NaCl crystals in drowning-out precipitation operation, *Trans IChemE Part A: Chem Eng Res Des*, 76: 809–814.

Tavare, N.S., 1995, Mixing, reaction, and precipitation—interaction by exchange with mean micromixing models, *AIChE J*, 41: 2537–2548.

Torbacke, M. and Rasmuson, A.C., 2004, Mesomixing in semi-batch reaction crystallization and influence of reactor size, *AIChE J*, 50: 3107–3119.

Ulrich, J. and Strege, C., 2002, Some aspects of the importance of metastable zone width and nucleation in industrial crystallizers, *J Crystal Growth*, 237: 2130–2135.

Wei, H.Y., Zhou, W. and Garside, J., 2001, Computational fluid dynamics modeling of the precipitation process in a semibatch crystallizer, *Ind Eng Chem Res*, 40(23): 5255–5261.

Woo, X.Y., Tan, R.B.H., Chow, P.S. and Braatz, R.D., 2006, Simulation of mixing effects in antisolvent crystallization using a coupled CFD-PDF-PBE approach, *Crystal Growth and Design*, 6(6): 1291–1303.

Yu, Z.Q., Tan, R.B.H. and Chow, P.S., 2005, Effects of operating conditions on agglomeration and habit of paracetamol crystals in anti-solvent crystallization, *J Crystal Growth,* 279: 477–487.

Yu, Z.Q., Chow, P.S. and Tan, R.B.H., 2006, Application of attenuated total reflectance-fourier transform infrared (ATR-FTIR) technique in the monitoring and control of anti-solvent crystallization, *Ind Eng Chem Res*, 45: 438–444.

Zauner, R. and Jones, A.G., 2002, On the influence of mixing on crystal precipitation processes – application of the segregated feed model, *Chem Eng Sci*, 57(5): 821–831.

The manuscript was received 27 October 2006 and accepted for publication after revision 11 March 2007.